Acta Crystallographica Section D
Biological Crystallography
ISSN 0907-4449

The three-dimensional structure of calcium-depleted human C-reactive protein from perfectly twinned crystals

Mohamed A. M. Ramadan,[a,b] Annette K. Shrive,[a] David Holden,[b]† Dean A. A. Myles,[b]‡ John E. Volanakis,[c] Larry J. DeLucas[d] and Trevor J. Greenhough[a]*

[a]School of Life Sciences, Keele University, Staffordshire ST5 5BG, England, [b]School of Chemistry and Physics, Keele University, Staffordshire ST5 5BG, England, [c]BSRC Alexander Fleming, 14-16 Fleming Street, Vari 166 72, Greece, and [d]University of Alabama at Birmingham, Birmingham, Alabama 35294, USA

† Present address: International Union of Crystallography, 5 Abbey Square, Chester CH1 2HU, England.
‡ Present address: EMBL Grenoble Outstation, 6 Rue Jules Horowitz, BP181, 38042 Grenoble CEDEX 9, France.

Correspondence e-mail: t.j.greenhough@keele.ac.uk

Received 21 October 2001
Accepted 27 March 2002

PDB Reference: C-reactive protein, 1lj7.

C-reactive protein is a member of the pentraxin family of oligomeric serum proteins which has been conserved through evolution, homologues having been found in every species in which they have been sought. Human C-reactive protein (hCRP) is the classical acute-phase reactant produced in large amounts in response to tissue damage and inflammation and is used almost universally as a clinical indicator of infection and inflammation. The role of hCRP in host defence and the calcium-dependent ligand-binding specificity of hCRP for phosphocholine moieties have long been recognized. In order to clarify the structural rearrangements associated with calcium binding, the reported affinity of calcium-depleted hCRP for polycations and other ligands, and the role of calcium in protection against denaturation and proteolysis, the structure of calcium-depleted hCRP has been determined by X-ray crystallography. Crystals of calcium-depleted hCRP are invariably twinned and those suitable for analysis are merohedral type II twins of point group 4 single crystals. The structure has been solved by molecular replacement using the calcium-bound hCRP structure [Shrive *et al.* (1996), *Nature Struct. Biol.* **3**, 346–354]. It reveals two independent pentamers which form a face-to-face decamer across a dyad near-parallel to the twinning twofold axis. Cycles of intensity deconvolution, density modification (tenfold NCS) and model building, eventually including refinement, give a final R factor of 0.19 ($R_{\rm free}$ = 0.20). Despite poor definition in some areas arising from the limited resolution of the data and from the twinning and disorder, the structure reveals the probable mode of twinning and the conformational changes, localized in one of the calcium-binding loops, which accompany calcium binding.

1. Introduction

C-reactive protein (CRP; Volanakis, 2001) is a member of the pentraxin family of oligomeric calcium-binding proteins. Homologues of CRP have been found in creatures as diverse as the phylogenetically ancient horseshoe crab and man (see, for example, Pepys *et al.*, 1978; Robey & Liu, 1981; Gewurz *et al.*, 1995; Jensen *et al.*, 1997; Lund & Olafsen, 1998; Shrive *et al.*, 1999). Human C-reactive protein (hCRP), a disc-like molecule consisting of five identical protomers of 206 amino acids arranged in a cyclic pentameric aggregation (Shrive, Cheetham *et al.*, 1996), is the classical acute-phase reactant produced in large amounts in response to tissue damage and inflammation and is used almost universally as a clinical indicator of infection and inflammation (Pepys & Berger, 2001). CRP's major physiological ligand, recognized in a calcium-dependent manner, is the phosphocholine (PC) head group exposed on damaged cells or foreign pathogens such as

pneumococcal C-polysaccharide (PnC; Volanakis & Kaplan, 1971). Following binding to PnC, but not to simple PC itself, hCRP binds C1q and efficiently activates complement (Volanakis, 1982). Although the primary biological function of CRP remains controversial, its functional activities and conservation suggest an important role in innate host defence.

Circular dichroism (Young & Williams, 1978; Mullenix & Mortensen, 1994), immunochemical (Kilpatrick *et al.*, 1982; Swanson *et al.*, 1991), infrared spectroscopy (Dong *et al.*, 1994) and other experiments (Heaton *et al.*, 1999) have suggested varying levels of hCRP conformational and/or allosteric change accompanying removal or binding of calcium. Since bound Ca^{2+} is required for PC binding, the calcium-induced conformational changes are generally reported to be essential for formation of the proper conformation of the phosphocholine-binding site (Kilpatrick *et al.*, 1982). Studies on the binding reactivity of hCRP for polycations (DiCamelli *et al.*, 1980; Potempa *et al.*, 1981; Dougherty *et al.*, 1982) show that polycation binding by both hCRP and rabbit CRP is inhibited by calcium, this inhibition being reversed by PC bound in the presence of calcium. These results have been interpreted in terms of proximal but distinct PC and polycation-binding sites, with calcium and polycations competing for the same site (Potempa *et al.*, 1981).

In addition to effecting the binding of physiological ligands, the calcium ions in hCRP also perform a role in maintaining the integrity of the protein. In the presence of calcium ions hCRP resists denaturation induced by high temperatures (Heaton *et al.*, 1999) and by high concentrations of urea (Potempa *et al.*, 1983). The binding of calcium to CRP may also serve to protect CRP from proteolytic degradation or denaturation in the blood during the acute phase of infection. In the absence of calcium, hCRP is cleaved between Asn145 and Phe146 by Nagarse protease, and between Phe146 and Glu147 by Pronase; this cleavage results in disruption of the two high-affinity calcium-binding sites (Kinoshita *et al.*, 1989). This cleavage is completely inhibited in the presence of 1 m*M* $CaCl_2$.

In the native calcium-bound hCRP structure (Shrive, Cheetham *et al.*, 1996) the protomers contain two calcium ions, both with a chelation of five. Each of the two independent pentamers within the crystal asymmetric unit contained a single protomer which forms a crystal contact with the calcium-binding site of a protomer from another pentamer, resulting in the loss of calcium within that protomer. Several changes in loops around the surface of the protomer, arising either from loss of calcium or from the crystal contacts were observed compared with the calcium-bound protomers. The two calcium ions per protomer form the binding site for the phosphate moiety of physiological ligands, including phosphocholine (PC). The structure of the hCRP–PC complex (Thompson *et al.*, 1999) shows that binding of simple PC produces no structural or conformational changes in either the protomer or the pentameric aggregate, leaving the hCRP structure (Shrive, Cheetham *et al.*, 1996) essentially unchanged. In order to clarify both the hCRP molecular conformational changes which accompany calcium binding and the affinity of calcium-depleted hCRP for polycations, the structure of calcium-depleted human CRP has been determined by X-ray crystallography.

2. Methods

2.1. Data collection and twinning

Human CRP was isolated from serum (Volanakis *et al.*, 1978) and crystallized according to DeLucas *et al.* (1987). Two tetragonal crystal forms (forms I and II) were grown in the absence of calcium, both with apparent point group 422. Data-collection and processing statistics have been reported previously (Myles *et al.*, 1990). Systematic absences and diffraction symmetry clearly suggest space group $P4_122$ or $P4_322$ for the form I crystals (unit-cell parameters a = 102, c = 309 Å) and space group $P4_222$ for the form II crystals (unit-cell parameters a = 103, c = 308 Å), with both crystal forms containing one pentamer within the asymmetric unit and 66% solvent (Myles *et al.*, 1990). Although the $R_{\rm sym}$ values clearly indicate point group 422 in both cases and no indication of twinning was detected by standard light microscopy, subsequent analysis has now shown both sets of data to be twinned (Holden, 1995). In the case of the form I crystals the apparently perfect 422 symmetry and the 4_1 absence indicate perfectly hemihedrally twinned crystals (twinning fraction $\alpha = 0.5$; Yeates, 1997) arising from $P4_1$ or $P4_3$ crystals twinned by 180° rotation about either [100] or [110]. These single crystals will thus contain two independent pentamers in the asymmetric unit. It is of interest to note that the intensity statistics [$N(Z)$ test] suggest a twinning fraction α = 0.25 (Holden, 1995). Model twins (Holden, 1995), the intensity statistics distribution function (Rees, 1980) and the structure solution, however, confirm α = 0.5 and the smoothing influence of high non-crystallographic symmetry on the intensity statistics, particularly for lower order reflections, leading to a reduction in the apparent α (Holden, 1995; Rees, 1980).

The form II crystals have been shown to be pseudo-merohedrally twinned (Holden, 1995) arising from $C222_1$ single crystals with unit-cell parameters a = 146, b = 145, c = 308 Å and a twinning fraction α = 0.5. In this case, a twofold rotation about the $C222_1$ [110] (equivalent to 90° about [001]) produces pseudo-tetragonal $P4_222$ crystals with apparent axes a = 103, c = 308 Å. Since $a \simeq b$ in the $C222_1$ lattice, small deviations from perfect overlap of the twin-related lattices are apparent in the diffraction pattern only at higher resolution. Single crystals of this calcium-free human CRP $C222_1$ crystal form (form III) have been obtained, but unresolved pseudosymmetry has so far prevented determination of the structure (Shrive, Holden *et al.*, 1996).

2.2. Structure determination

The calcium-free structure was determined from the form I crystals by molecular replacement using the calcium-bound structure of human CRP (Shrive, Cheetham *et al.*, 1996) and programs from the *CCP*4 suite (Collaborative Computational Project, Number 4, 1994) and *X-PLOR* (Brünger, 1992). The

diffraction data were collected on film in 1989 and the only data now available are those merged in 422. The self-rotation function calculated in $P422$ gave a single fivefold direction (Yeates, 1997) at $\varphi = 45, = 57, \kappa = 72^\circ$ (Myles *et al.*, 1990). As the pentamers in the calcium-bound structure contained one protomer in each pentamer which contained no calcium and differed slightly in conformation to the other protomers, a model pentamer consisting of five identical calcium-bound protomers was used for molecular-replacement studies. The pentamer was aligned with the pentameric fivefold along tetragonal *c*. Cross rotation functions (*ALMN*) using the twinned data in 422 gave a single outstanding solution (rotation R_1) at $\alpha = 45$, $\beta = 57$, $\gamma = 64^\circ$ which corresponds to the expected fivefold direction from self-rotation functions. As expected, cross rotation-function studies on the twinned data expanded to $P4$ symmetry gave the two fivefold directions R_1 at $\alpha = 45$, $\beta = 57$, $\gamma = 64^\circ$ and R_2 at $\alpha = 45$, $\beta = 123$, $\gamma = 28^\circ$, which are twofold-symmetry related in 422 about [110] when the equivalents of R_1 at $\alpha = 135$, $\beta = -57$, $\gamma = -116^\circ$ and of R_2 at $\alpha = 135$, $\beta = 123$, $\gamma = 28^\circ$ are used. Translation-function searches were carried out on the twinned data expanded to $P4$ symmetry. The rotation-function solution R_1 gave two outstanding translations (heights 24 r.m.s.; *TFFC*) in $P4_3$: T_{11} at $x = 0.204$, $y = 0.970$, $z = 0.0$ and T_{12} at $x = 0.243$, $y = 0.928$, $z = 0.0$. Solutions in $P4_1$ were at a significantly lower level (10 r.m.s.). The twofold-related orientation R_2, an independent rotation in $P4$ and part of the crystal symmetry in point group 422, gave the two expected outstanding solutions, which were related to T_{11} and T_{12} by the twinning twofold parallel to [110], in $P4_3$: T_{21} at $x = 0.928$, $y = 0.243$, $z = 0.0$ and T_{22} at $x = 0.971$, $y = 0.204$, $z = 0.0$. Inputting solution R_1T_{11} gave the translation for R_2 as $T_{21} = 0.429, 0.743, 0.068$ (at 50 r.m.s.) and inputting R_1T_{12} gave the translation for R_2 as $T_{22} = 0.469, 0.704, 0.068$ (at 49 r.m.s.) and *vice versa*. This therefore gives two pairs of solutions, the pair R_1T_{11}, R_2T_{21} and its twin-related pair R_2T_{22}, R_1T_{12}, related by the twinning twofold which generates 422 symmetry through interaction with the tetragonal fourfold. We therefore have two solutions, designated Single and Twin, one from each of the two twin-related portions of the crystal. Since R_1 and R_2 are twofold related about the twinning twofold in the crystal, each of the twin-related portions also contains a twofold, relating R_1T_{11} and R_2T_{21} for the Single portion and necessarily defined as parallel to [110] at this stage, but in this case it occurs as twofold NCS. Packing diagrams revealed that the two independent pentamers in $P4_3$ were assembled to form decamers with 52 NCS symmetry, one of the decameric NCS twofolds being that parallel to [110] and hence the twinning twofold (see §3). While the solutions chosen define the twinning twofold as parallel to [110], choice of other symmetry-equivalent rotations would have provided an equally valid twinning twofold parallel to $[1\bar{1}0]$.

The fit of the starting model to the observed twinned data $I_{\rm obs}$, expanded to $P4_3$, was investigated by scaling $I_{\rm obs}$ to the combined calculated $P4_3$ intensities for the solution (structure factor $|F_c|_{\rm Single}$) and its twin (structure factor $|F_c|_{\rm Twin}$). $|F_c|_{\rm Single}$ was calculated from the solution pair R_1T_{11} (protomers *A*, *B*, *C*, *D*, *E*) and R_2T_{21} (protomers *F*, *G*, *H*, *I*, *J*), and the twin-related structure factor $|F_c|_{\rm Twin}$ was calculated by reindexing of $|F_c|_{\rm Single}$ by $hkl \Rightarrow kh\bar{l}$ (equivalent to a twofold rotation about [110]). Conversion to intensities and placement in the $P4_3$ asymmetric unit was followed by calculation of $I_{c\rm Single+Twin} = \alpha I_{c\rm Single} + (1 - \alpha)I_{c\rm Twin}$ and scaling to the observed twinned data $I_{\rm obs}$. A scaling R factor $R_{s\rm Single+Twin} = \sum \big||F_c|_{\rm Single+Twin} - |F_{\rm obs}|\big| / \sum |F_{\rm obs}|$ (*SCALEIT*) of 0.335 for $\alpha = 0.5$ was obtained. The merging of the observed data in 422 imposes a minimum value of $R_{s\rm Single+Twin}$ at $\alpha = 0.5$.

Following an initial rigid-body refinement (*X-PLOR*) of the Single solution R_1T_{11}, R_2T_{21} (calculated structure factor $|F_c|_{\rm Single}$) against the twinned observed data $|F_{\rm obs}|$ expanded to $P4_3$, the scaling R factor $R_{s\rm Single+Twin}$ was reduced to 0.259. The rigid-body refinement itself gave an R factor ($R = \sum \big||F_c|_{\rm Single} - |F_{\rm obs}|\big| / \sum |F_{\rm obs}|$) of 0.348 from the initial value of 0.387, using all data in the resolution range 20–3.15 Å. The final rotations and translations of the refined rigid-body model relative to the starting model were $\alpha = 134.8$, $\beta = -58.0$, $\gamma = -115.6^\circ$; $x = 0.204$, $y = 0.971$, $z = 0.000$ for R_1T_{11} and $\alpha = 134.3$, $\beta = 122.3$, $\gamma = 28.5^\circ$; $x = 0.430$, $y = 0.743$, $z = 0.068$ for R_2T_{21}. The refined values of R_1 and R_2 suggest that the NCS twofold relating R_1T_{11} and R_2T_{21} deviates slightly from parallel to [110].

2.3. Model building and refinement

The general procedure now followed throughout the structure solution and refinement was as follows: the Single solution pair R_1T_{11}, R_2T_{21} in $P4_3$ was used as the model for building and for the subsequent generation of $F_{c\rm Single}$ (*SFALL*) and hence $I_{c\rm Single}$ and, by reindexing (*REINDEX*), the twin-related intensity $I_{c\rm Twin}$. $|F_o|_{\rm Single}$ was then calculated according to Redinbo & Yeates (1993),

$$|F_o|_{\rm Single} = (I_{o\rm Single})^{1/2} = [(I_{\rm obs} + I_{c\rm Single} - I_{c\rm Twin})/2]^{1/2}.$$

Each cycle of model building ($2|F_o|_{\rm Single} - |F_c|_{\rm Single}$ maps in *O*) was followed by recalculation of $|F_c|_{\rm Single}$, $\varphi_{c\rm Single}$ and $|F_o|_{\rm Single}$ (*SFALL*, *SIGMAA*), followed by density modification, tenfold NCS averaging (*DM*) and calculation of a new Fourier map (*FFT*). The progress of the structural refinement and of the detwinning procedure for $|F_o|_{\rm Single}$ was monitored by scaling of $|F_c|_{\rm Single}$ to $|F_o|_{\rm Single}$ (*RSTATS*; 20–3.15 Å data) and calculation of the scaling R factor $R_{s\rm Single} = \sum \big||F_c|_{\rm Single} - |F_o|_{\rm Single}\big| / \sum |F_o|_{\rm Single}$. The initial value of $R_{s\rm Single}$ was 0.223.

Prior to the first cycle of model building, $2|F_o|_{\rm Single} - |F_c|_{\rm Single}$ Fourier maps with various regions of the structure (including the pentraxin helix) omitted from $F_{c\rm Single}$ and from the NCS protein mask in *DM* clearly showed the omitted regions, confirming the initial quality and independence of the maps. These maps also showed significant structural change in the calcium-binding loop 138–150 and various conformations of this loop, where visible, in different protomers. The conformation of residues 57 and 58 was also seen to vary between the protomers owing to contacts with the 138–150 loop; the appropriate residues in the appropriate protomers were subsequently omitted from all averaging procedures.

Additional residues not conforming to the NCS were removed from averaging as the structure refinement progressed. Following four cycles of model building, recalculation of $|F_o|_{\rm Single}$, NCS averaging and density modification, the scaling R factor $R_{s\rm Single}$ was reduced to 0.219 for all data in the resolution range 20–3.15 Å. A rigid-body refinement (*X-PLOR*) of the resulting 'Single' model (calculated structure factor $|F_c|_{\rm Single}$) against $|F_o|_{\rm Single}$ reduced the scaling R factor $R_{s\rm Single}$ to 0.215. The rigid-body refinement itself gave an R factor ($R = \sum \big||F_c|_{\rm Single} - |F_o|_{\rm Single}\big| / \sum |F_o|_{\rm Single}$) of 0.224 using all data in the resolution range 20–3.15 Å.

The free R factor was not used up to this point and indeed it is open to some debate as to whether such a quantity is truly meaningful when both $|F_{\rm obs}|$ and $F_{\rm calc}$ are altered at each stage of structure solution and refinement. Nevertheless, since the free R will provide an independent check for a given set of $|F_{\rm obs}|$ during a multiple-cycle refinement pass, a free R set (5% of the reflections) was generated prior to *X-PLOR* refinement and was maintained throughout the remainder of the refinement. Cycles of calculation of $|F_o|_{\rm Single}$, *X-PLOR* positional refinement using tenfold NCS restraints where appropriate, recalculation of $|F_o|_{\rm Single}$, density modification, symmetry averaging, map calculation and model building were carried out. This procedure reduced the R factor in *X-PLOR* ($R_{\rm Xplor} = \sum \big||F_c|_{\rm Single} - |F_o|_{\rm Single}\big| / \sum |F_o|_{\rm Single}$) from an initial value of 0.224 ($R_{\rm Xplor\,free} = 0.223$) to 0.219 (0.219), respectively. The value of $R_{s\rm Single}$ at this stage was 0.218. The *X-PLOR* component of the structure refinement was extended to include cycles of overall B-factor refinement (which converged to $B = 20.8$ Å^2) followed by individual B-factor refinement. NCS restraints were applied throughout as appropriate. The final R factors were $R_{s\rm Single} = 0.188$, $R_{\rm Xplor} = 0.186$ and $R_{\rm Xplor\,free} = 0.199$ for all data between 20 and 3.15 Å. All main-chain and side-chain stereochemical parameters fall either inside or are better than those expected from a structure at 3.15 Å resolution (*PROCHECK*; Laskowski *et al.*, 1993), with 77% of the residues in the most favoured regions of the Ramachandran plot and 23% in additional allowed regions. There are four residues in generously allowed regions and none in disallowed regions. It has not been

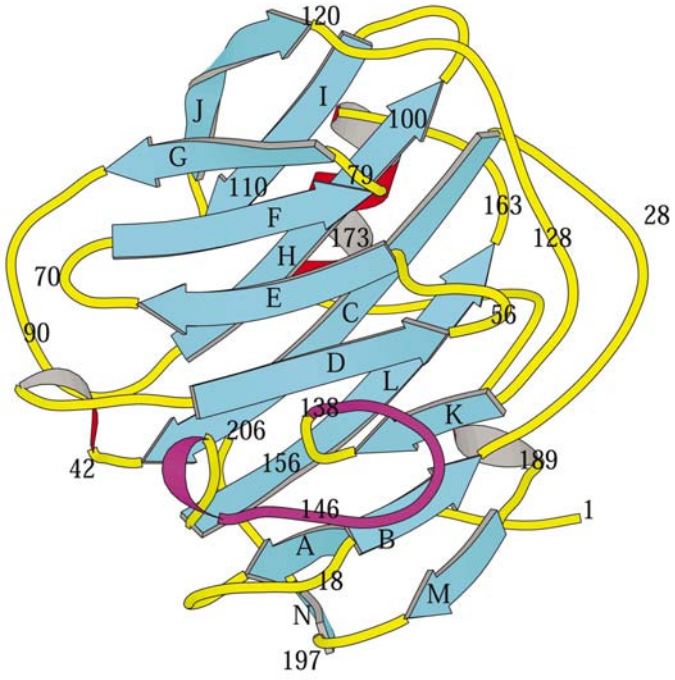

Figure 1
The calcium-depleted human CRP protomer (generated using *MOLSCRIPT*; Kraulis, 1991). The entire calcium-binding loop 138–150, shown in purple, is ordered in the protomer shown (protomer *J*). A small subset of the residues are numbered to clarify references to particular regions and residues in the text.

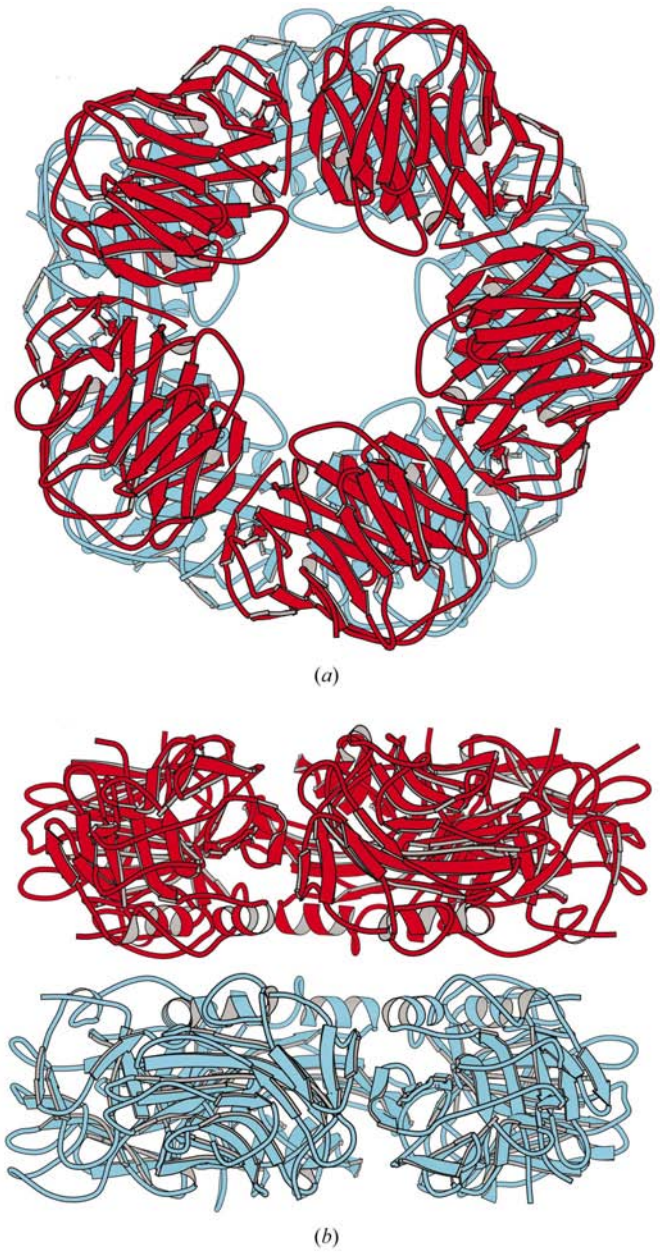

Figure 2
The calcium-depleted human CRP decamer (generated using *MOLSCRIPT*; Kraulis, 1991). (*a*) Viewed down the molecular fivefold, (*b*) viewed down one of the NCS twofolds.

possible to alleviate a small number of relatively short bad contacts, mainly involving residues either directly or indirectly involved in crystal packing and twinning (see §4).

3. Results

3.1. Overall structure

The 3.15 Å structure reveals the pentraxin fold (Fig. 1) and two independent pentamers, P_1 composed of protomers *A*, *B*, *C*, *D*, *E* and P_2 composed of protomers *F*, *G*, *H*, *I*, *J*, which form a face-to-face (pentraxin helix to pentraxin helix) NCS 52 point-group symmetry decamer with the two pentameric fivefold axes coincident (Fig. 2). The relative rotation between P_1 and P_2, as defined by the difference between the centres of mass of the subunits in the two pentamers, is approximately 20° and the calcium-binding regions are situated on the two external pentameric faces of the decamer. The fivefold approximately symmetrical (at this resolution) contact between the two pentamers in the decamer is made by the pentraxin helix (169–176) and the 'jug-handle' loop 177–182 which immediately follows the pentraxin helix and shows local conformational changes with respect to the native calcium-bound structure (Shrive, Cheetham *et al.*, 1996). The contact residues are Thr173 in P_1 and Pro179 in P_2 and *vice versa*, the decamer thus being stabilized by five relatively small surface contacts between the two pentamers.

The decameric NCS twofold near-perpendicular to *z* in the layer of pentamers at $z = 0$ (Fig. 3) is near-parallel to [110] and approximately bisects the *a* and *b* axes (see below) and relates protomer pairs *AI*, *BJ*, *CF*, *DG* and *EH*. This NCS twofold is thus near-parallel to the twinning twofold axis parallel to [110] (see §4). Significant deviations (at this resolution) from the NCS are seen only in regions involved in and proximal to the contact interfaces both between and within the *z* layers of decamers. A least-squares fit of the two pentamers across the NCS twofold, based on C^{α} atoms and excluding contact regions, gives an r.m.s. deviation of 0.3 Å and direction cosines of the NCS twofold corresponding to 45.3° from *a*, 44.7° from *b* and 89.4° from *c*. The NCS twofold is thus 0.6° from [110]. The major significant conformational change between the calcium-depleted and the calcium-bound protomer structure (Shrive, Cheetham *et al.*, 1996) is shown by the calcium-binding loop 138–150 (L_1). Substantial parts of this loop are disordered and mobile except in protomers *B*, *F*, *G* and *J* (see Fig. 4), where it makes a crystal contact within a *z* layer (the decamers related by unit-cell translations perpendicular to *z*)

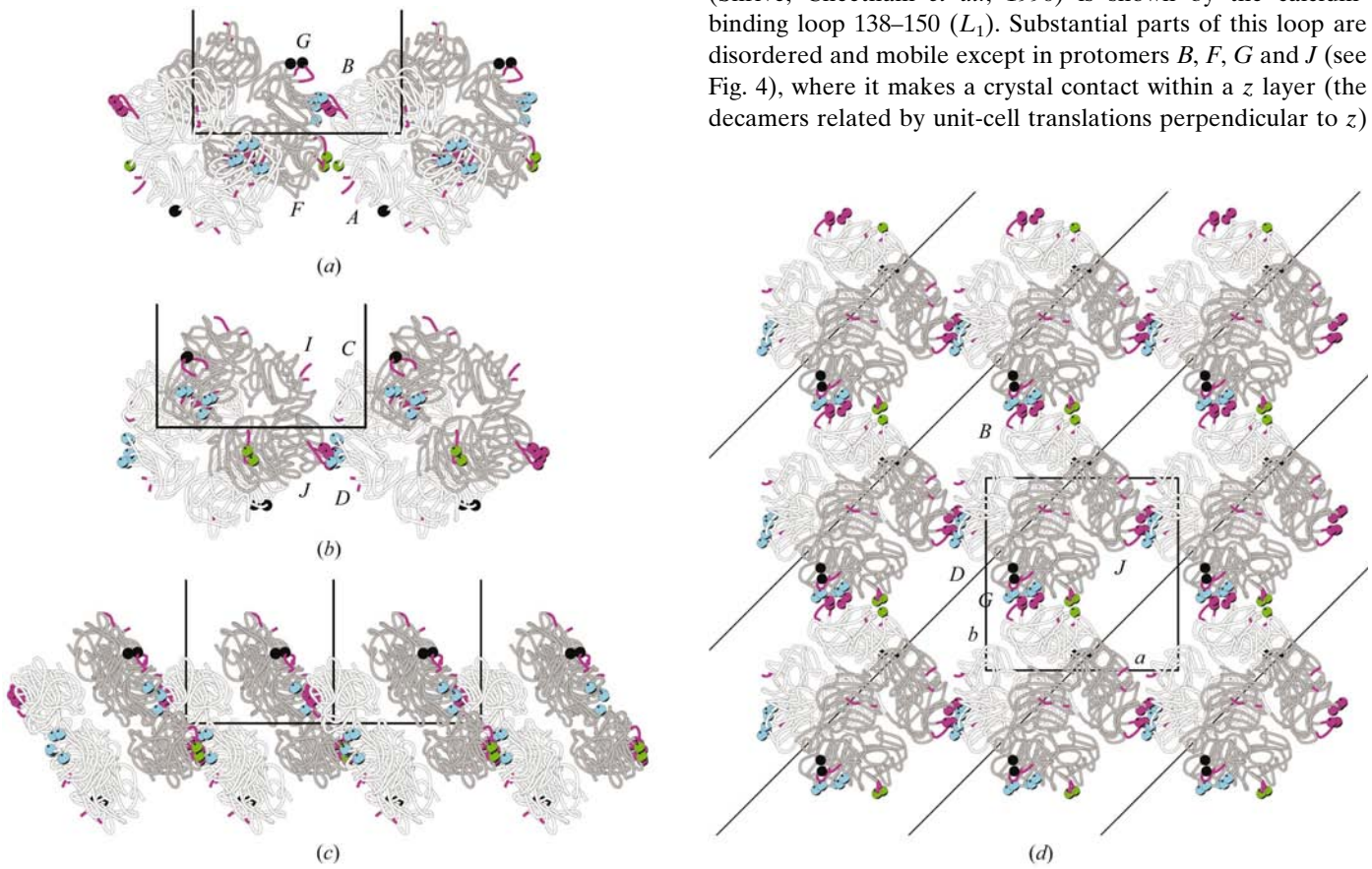

Figure 3
Arrangement of the hCRP decamers within a layer of *z*. The layer at $z = 0$ is shown with the *A*–*E* pentamer in white and the *F*–*J* pentamer in grey. The calcium-binding loop 138–150 is in magenta and residues involved in crystal packing are shown as spheres, with interlayer contacts in black. The major intra-layer packing interactions are between protomers *J* (magenta) and *D* (cyan) and protomers *B* (magenta) and *G* (cyan), *B* and *G* being twofold NCS-related to *J* and *D*, respectively. The contact between subunits *F* and *A* is shown in green. (*a*) View down [100]; (*b*) view down [010]; (*c*) view down [110], approximately parallel to the NCS twofold axis; (*d*) view down [001] showing the direction of the NCS twofold which passes through the decameric centre and is approximately parallel to the [110] direction. Owing to the deviation (not shown) of the NCS twofold from parallel to [110], the *JD* and *BG* interfaces are not exactly equivalent and the NCS equivalent of the interaction between subunits *F* and *A* (NCS-related to *C* and *I*, respectively) is not present. Figure generated using *MOLSCRIPT* (Kraulis, 1991).

for protomers *B*, *J* and *F*, and between layers for protomer *G*. The twofold NCS-related protomer pair P_1B and P_2J from one decamer make extensive contacts [through $L_1B(J)$ and loop $L_2B(J)$ residues 57–60] with the twofold NCS-related protomer pair P_2G and P_1D, respectively, in decamers translated by *b* (protomer *G*) and *a* (protomer *D*), these contacts being propagated by unit-cell translations throughout each layer in *z* (see Fig. 3). The contacts at these intra-layer interfaces are formed by $L_1B(J)$ with L_2 (57–60)$G(D)$ and L_3 (122–125)$G(D)$, and L_2 (57–60)$B(J)$ with L_3 (122–125)$G(D)$ and L_4 (80–81)$G(D)$ (Fig. 5). The small 0.6° deviation of the NCS twofold from parallel to [110] (in the $z \simeq 0$ layer) results in non-equivalence of these two major contact interfaces (see below). L_1F and L_1G are also ordered, but entirely different from $L_1B(J)$ and each other, making contacts as part of the interaction within (L_1F) and between (L_1G) the layers in *z*. Many of these intra-layer contacts are difficult to define despite reasonable electron density in most cases. This is not surprising in view of the limited resolution, the probable mode of twinning (see below) and exclusion from the NCS. The few contacts which exist between the *z* layers are non-specific and are generally poorly defined by the density. These contacts, which all involve protomer *A*, are between Tyr125*A* and Asn145*G* (3.3–3.6 Å), Lys122*A* and Thr17*G* (Thr17*G* OG1–Lys122*A* CE, 3.14 Å) and Asp70*A* and Tyr125*H* (>3.6 Å). Protomers *C*, *E* and *I* make no packing contacts and loop L_1 is disordered and without clear density in these protomers and in protomers *A*, *D* and *H*.

4. Discussion

4.1. Conformational changes and calcium binding

The loss or addition of calcium does not induce significant allosteric or conformational changes either in the pentameric aggregation or the protomer except in the mobile calcium-binding loop L_1. This 138–150 loop contains glycine residues at 143 and 144, as do all known pentraxin sequences, and a third glycine at residue 148 which, of the sequenced vertebrate pentraxins, is unique to human CRP. Although the calcium-binding loop L_1 adopts variable conformations in the crystal structure, with the reasonably well defined examples in protomers *B*, *F*, *G* and *J* (see Fig. 4) arising from crystal contacts, it is more likely that this loop is generally mobile, as in the remaining protomers, in the absence of bound calcium. Indeed, the crystal contacts appear to define the conformations seen in the visible loops L_1, with L_1B and L_1J having similar contacts and closely similar conformations, while L_1F and L_1G have entirely different contacts and conformations both to each other and to L_1B and L_1J. On calcium binding, which is necessary for both access and binding of phosphocholine-containing ligands, the glycine-rich loop L_1 folds in to protect the protease-sensitive site (Asn145–Glu147) from proteolytic attack (Kinoshita *et al.*, 1989), with Glu147 coordinating to one of the calcium ions (Shrive, Cheetham *et al.*, 1996). CD (Young & Williams, 1978; Mullenix & Mortensen, 1994), immunochemical (Kilpatrick *et al.*, 1982; Swanson *et al.*,

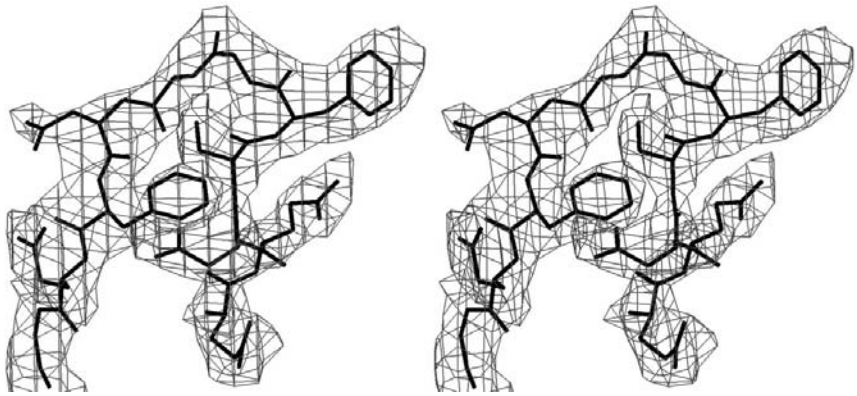

Figure 4
Stereoview of the ordered calcium-binding loop L_1 in protomer *B*. Residues 138–148 are shown. Electron density is contoured at 1 r.m.s.d.

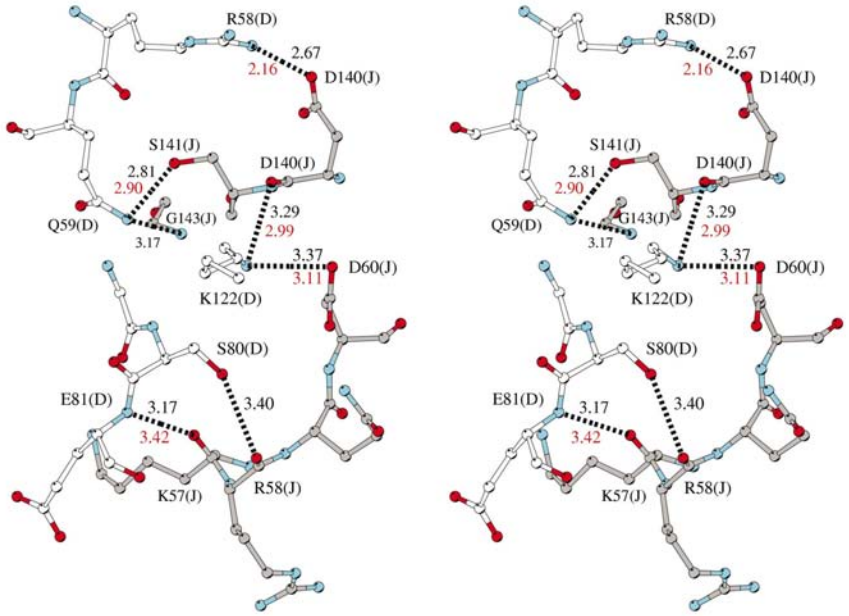

Figure 5
The extensive intra-layer crystal-packing contact between protomers *J* and *D* (distances in black) in decamers related by unit-cell translations in *a*. The contact between protomers *B* and *G*, NCS-related to protomers *J* and *D*, respectively, occurs between decamers related by unit-cell translations in *b* (distances in red). Figure generated using *MOLSCRIPT* (Kraulis, 1991).

1991) and infrared spectroscopy (Dong *et al.*, 1994) experiments have been interpreted in terms of large conformational and/or allosteric changes upon removal or binding of calcium. The structural results presented here show only mobility in the calcium-binding loop L_1, while the spectroscopic results, for example, have been interpreted as indicating significant increases in both β-sheet and helical content on calcium binding (Dong *et al.*, 1994). Disorder in the calcium-binding loop 138–150 has been observed in other pentraxin protomers which lack calcium (Shrive, Cheetham *et al.*, 1996), but the results presented here show that the associated conformational changes observed in other loop regions in the calcium-depleted protomer of our previously reported structure arise not from loss of calcium itself, but from crystal-packing interactions. These interactions produce chelation of the 138–150 loop in the calcium-depleted protomer into one of the calcium- and phosphocholine-binding sites of a neighbouring pentamer in the crystal, leading to loss of the Arg47 to main-chain Ser149 and Ser151 hydrogen bonds and significant movement of the 43–48, 68–72 and 85–91 loops (Shrive, Cheetham *et al.*, 1996). These hydrogen bonds are intact in the present structure and there is no significant movement in any of the three loops. In two of the ten independent protomers in the native calcium-bound protomers, a crystal contact between Glu147 and Arg58 in a neighbouring protomer results in a low-occupancy calcium site in these two protomers (Shrive, Cheetham *et al.*, 1996), although L_1 is still correctly folded in for calcium binding.

4.2. The decamer in the crystal

Despite many attempts using various NCS combinations during refinement and repeated model building, the ten van der Waals contacts across the decameric interface could not be equalized. The contacts between protomers *AJ* and *CH* could not be extended beyond 3.1 Å, while all others were 3.3 Å or greater. While this may suggest small deviations from 52 symmetry, the electron density at this resolution is relatively poor, a situation exacerbated by the twinning (see below). The decamer formation and the associated local conformational changes are probably a consequence of crystal packing, although other calcium-depleted human CRP crystal forms do appear to contain similar decamers (Shrive, Holden *et al.*, 1996). Two pentamers of the homologous human serum amyloid P-component (hSAP) complexed with the ligand 2′-deoxyadenosine-5′-monophosphate (dAMP) aggregate in the crystal through dAMP–dAMP interactions to form a decamer with the calcium-binding pentameric faces forming the decameric interface (Hohenester *et al.*, 1997). While recent results suggest that human hSAP is a single uncomplexed pentamer in whole serum (Hutchinson *et al.*, 2000), X-ray and neutron scattering results combined with molecular modelling (Ashton *et al.*, 1997) suggest that native calcium-bound hSAP aggregates to form a physiological helix-to-helix decamer very similar to that reported here but perhaps with a relative rotation of 36° between P_1 and P_2. Despite the high sequence and structural homology between hSAP and hCRP, the relative protomer orientation within the pentameric aggregate

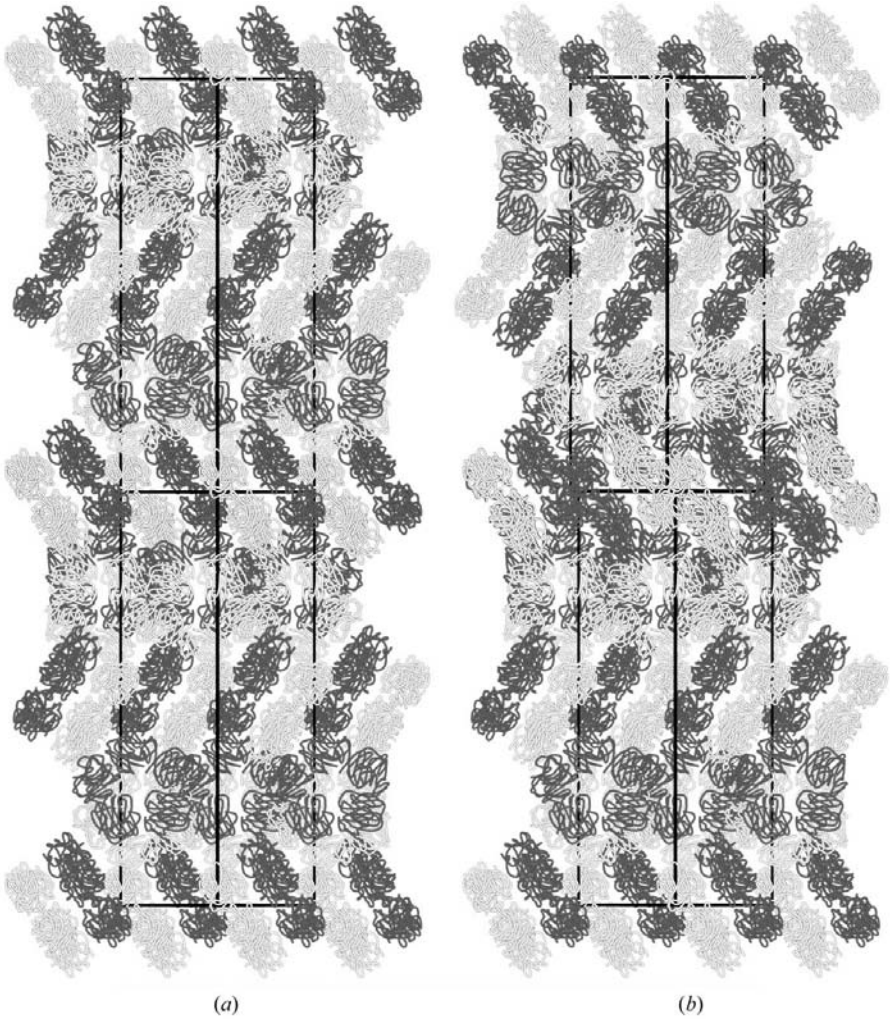

Figure 6
(*a*) View of the packing of hCRP in $P4_3$ viewed down [110], approximately parallel to the NCS twofold direction in the layer at $z = 0$. Two unit cells, one from each of two identical domains, are shown overlaying at the domain interface. The *A*–*E* pentamer is in white and the *F*–*J* pentamer in grey, with the *c* axis vertical. (*b*) Representation of a possible twinning model showing two unit cells, one from each of two twinned domains, overlaid at the domain interface. The view is down [110], approximately parallel to the NCS twofold direction in the layer at $z = 0$. The second (uppermost) domain is related to the lower domain by the twinning twofold parallel to [110]. The two domains have been overlaid at the interface but will not overlay exactly as the NCS twofold is not exactly parallel to [110]. Figure generated using *MOLSCRIPT* (Kraulis, 1991).

differs by 14° (Shrive, Holden *et al.*, 1996). Furthermore, the conformation of the 'jug-handle' loop 177–182 differs markedly between the two pentraxins (Shrive, Cheetham *et al.*, 1996) and Thr173 in hCRP is serine in hSAP. The crystal contact in calcium-depleted hCRP revealed here (Pro179–Thr173) and the nature of the resulting decameric structure are thus unlikely to be reflected in the decameric form of hSAP.

4.3. Crystal packing and twinning

In considering and visualizing the twinning and its relationship to the NCS, it is convenient to translate the asymmetric unit decamer centre to $z = 0$ and to consider this decamer and the other decamers in that z layer related by unit-cell translations in a and b (Fig. 3). These decamers contain an NCS twofold which is approximately perpendicular to z and near-parallel to [110] and which approximately bisects the a and b axes (Fig. 3*c*). Since the diffraction pattern exhibits perfect (at this resolution) 422 symmetry, the twinning twofold is necessarily parallel to but not necessarily coincident with (in this case) the [110] direction. Any significant angular deviation from parallel to [110] would produce two visibly distinct (split spots) rather than a single (overlaid spots) diffraction pattern.

In this tetragonal system, a strictly parallel relationship between the decameric NCS twofold and [110] would give non-crystallographic symmetry extending throughout the crystal within each layer of z (see Fig. 3), any deviations arising from contacts between layers. The contacts within each layer (protomer *B* to protomer *G* and *D* to *J*) would then be NCS-related, with the *BG* and *DJ* interfaces essentially identical. A small deviation of the NCS twofold from parallel to [110] is revealed by the calculated direction of the NCS dyad (0.6° from [110]) and by the non-equivalence of the *BG* and *JD* intra-layer contact interfaces formed by the NCS-related protomer pairs *BJ* and *GD*. This deviation is further evidenced by the ordered L_1F loop and the L_1F (Asn145) contact with Thr17*A* in a neighbouring decamer (see Fig. 3). This contact is also within the z layers but the NCS-related L_1C (145)–17*I* contact is not present, L_1C being disordered with no coherent density.

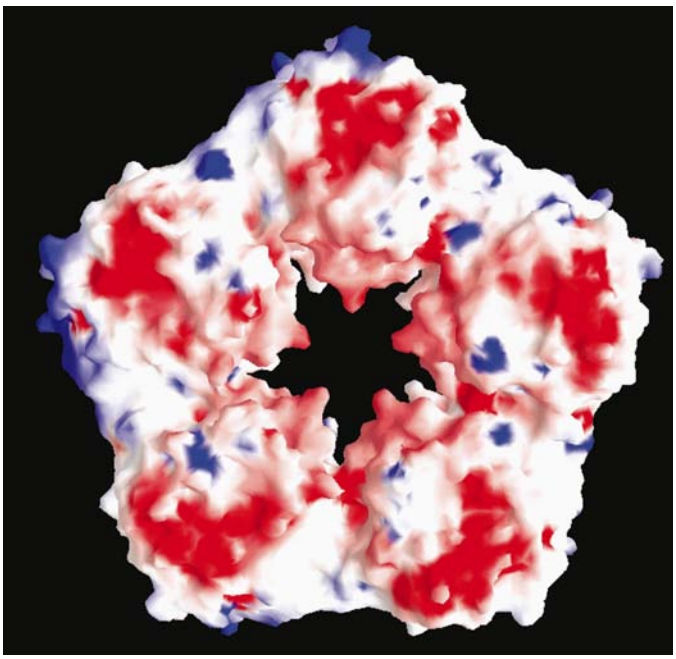

Figure 7
GRASP (Nicholls & Honig, 1992) surface-charge representation of the calcium-depleted human CRP pentamer. The highly negative region corresponds to the calcium- and ligand-binding region. In order to visualize the charge distribution, the ordered loop from protomer *J* has been included in all protomers.

The propensity of the crystals to invariably form apparently perfect twins suggests a parallel or near-parallel relationship between the twinning twofold and an NCS twofold such that the twin is locally near-identical, owing to the NCS, to the original structure in terms of the three-dimensional arrangement of the decamers within a z layer. The structure solution confirms this relationship, with the NCS twofold approximately perpendicular to z being near-parallel to the twinning [110] twofold. The twinned crystal can then be most easily viewed (although there are many other equivalent scenarios) as consisting of two halves related by a twinning twofold parallel to [110], the z layer at the interface being a part of one of the halves but with each of the decamers in this layer being related by twofold NCS (approximately parallel to [110]) to the decamer it replaces in the other half (see Fig. 6). As the NCS dyad and the twinning axis are not exactly parallel, this mode of twinning would give rise to structural perturbations at and either side of the twinning interface. The difficulties in establishing good geometry for the intra-layer contacts, and to a lesser extent the inter-layer contacts, suggests that this is indeed the case, with the crystal being composed of multiple twinned regions such that the perturbed contacts at the twinning interfaces are a significant component of the average structure. The decamers at the twinning interface, rather than being correctly aligned to the structure on one side of the interface, may adopt an intermediate conformation with the NCS dyad strictly parallel to [110], such that the layer is equally disposed to the twin-related regions either side of the interface. The weak diffraction to only medium resolution perhaps reflects this disorder. A further consequence of the non-coincidence of the NCS twofold with the line which bisects the a and b axes (Fig. 3*c*) is that this proposed mode of twinning would give rise to a translation in the $[\bar{1}10]$ (or $[1\bar{1}0]$) direction between the two 'halves' of the crystal (Fig. 6). This translation arises from the shift (calculated as 5.8 Å) between the two twin-related pairs of solutions from the rotation and translation functions.

4.4. Ligand binding

In the native structure the first calcium ion is coordinated by Asp60, Asn61, Glu138, Asp140 and the main-chain carbonyl of Gln139, and the second by Glu138, Asp140, Glu147 (×2) and Gln150 (Shrive, Cheetham *et al.*, 1996). The loss of calcium results in the highly negatively charged content of the loop L_1 region (Glu138, Gln139, Asp140, Asn145, Glu147,

Gln150) no longer being directed towards the calcium ions but being positioned and available for external interaction (Fig. 7). Glu81, which interacts with the positively charged quaternary amine in the PC-bound structure (Thompson *et al.*, 1999), and the calcium coordinators Asp60 and Asn61 are also available for external interaction. This major change in the electrostatic surface is of significance to binding studies on calcium-depleted hCRP. hCRP has been shown to exhibit affinity for polycations only in the absence of calcium or the presence of calcium and bound PC. The externally available Asp60, Asn61, Glu81 and the highly polarized loop L_1 in the calcium-depleted structure are prime candidates for polycation binding. The affinity of calcium-bound, PC-complexed hCRP for polycations may simply reflect a charge–charge interaction between the phosphate moiety and polycation ligands. The crystal contacts in the calcium-depleted structure reveal how interaction with positively charged residues in polycation ligands such as poly-L-lysine (DiCamelli *et al.*, 1980; Potempa *et al.*, 1981) may occur. The calcium-depleted hCRP–polycation interaction is mimicked by the crystal contacts of $L_2G(D)$ (through Arg58 and Gln59) with $L_1B(J)$ (Asp140 and Ser141) and $L_3G(D)$ (through Lys122) with $L_2B(J)$ (Asp60) (see Fig. 5).

5. Conclusions

Structural studies of human CRP now provide a full description of the structural basis of calcium binding and of binding to PC (Shrive, Cheetham *et al.*, 1996; Thompson *et al.*, 1999), while structural and related studies have defined the topology and structure of the binding site for complement component C1q (Agrawal *et al.*, 2001). C1q binding and complement activation by hCRP requires ligand-complexed hCRP and it is now clear that conjugated PC, *e.g.* PnC, rather than simple PC is required (Szalai *et al.*, 1999). Indeed, binding of simple PC produces no significant changes in either the protomeric or pentameric structure (Thompson *et al.*, 1999). Whether there are structural changes arising from binding of conjugated PC, transmitted around the surface of the protomer to the C1q site (Agrawal *et al.*, 2001) through a series of three loops (Shrive, Cheetham *et al.*, 1996) or by protomer tilt, or whether there is direct interaction between C1q and the bound polysaccharide tail, is not yet clear.

The present study reveals how the presence of calcium produces conformational changes which lead to increased stability of human CRP and to the formation of the binding site for the PC head group of physiological ligands. The position of Glu147, which is Asp in hSAP and does not extend into the calcium-binding pocket, appears to be critical for the binding affinity for the second calcium ion in hCRP. Low calcium concentrations may lead to not only reduced affinity for physiological PC ligands, but also to movement of the 138–150 loop, resulting in increased susceptibility to proteolysis and denaturation. The availability of this loop for external interaction may also give rise to a binding affinity for polycations including physiological lysine- and arginine-rich ligands. Through the 138–150 loop, calcium ion concentration plays a dual role in controlling both the biological activity and the stability of human CRP.

This work was supported in part by grants from the Medical Research Council, UK (to TJG) and from the Egyptian Educational and Cultural Bureau (to MAMR).

References

Agrawal, A., Shrive, A. K., Greenhough, T. J. & Volanakis, J. E. (2001). *J. Immunol.* **160**, 3998–4004.
Ashton, A. W., Boehm, M. K., Gallimore, J. R., Pepys, M. B. & Perkins, S. J. (1997). *J. Mol. Biol.* **272**, 408–422.
Brünger, A. T. (1992). *X-PLOR Manual, Version 3.1.* Yale University, New Haven, CT, USA.
Collaborative Computational Project, Number 4 (1994). *Acta Cryst.* D**50**, 760–763.
DeLucas, L. J., Greenhough, T. J., Rule, S. A., Myles, D. A. A., Babu, Y. S., Volanakis, J. E. & Bugg, C. E. (1987). *J. Mol. Biol.* **196**, 741–742.
DiCamelli, R., Potempa, L. A., Siegel, J., Suyehira, L., Petras, K. & Gewurz, H. (1980). *J. Immunol.* **125**, 1933–1938.
Dong, A., Caughey, W. S. & DuClos, T. W. (1994). *J. Biol. Chem.* **269**, 6424–6430.
Dougherty, T., Potempa, L. A., Gewurz, H. & Siegel, J. (1982). *Ann. NY Acad. Sci.* **389**, 444–445.
Gewurz, H., Zhang, X.-H. & Lint, T. F. (1995). *Curr. Opin. Immunol.* **7**, 54–64.
Heaton, R. J., Raynes, J. G. & Johnston, D. S. (1999). *Thermochim. Acta*, **334**, 97–106.
Hohenester, E., Hutchinson, W. L., Pepys, M. B. & Wood, S. P. (1997). *J. Mol. Biol.* **269**, 570–578.
Holden, D. (1995). PhD thesis, Keele University, England.
Hutchinson, W. L., Hohenester, E. & Pepys, M. B. (2000). *Mol. Med.* **6**, 482–493.
Jensen, L. E., Hiney, M. P., Shields, D. C., Uhlar, C. M., Lindsay, A. J. & Whitehead, A. S. (1997). *J. Immunol.* **158**, 384–392.
Kilpatrick, J. M., Kearney, J. F. & Volanakis, J. E. (1982). *Mol. Immunol.* **19**, 1159–1165.
Kinoshita, C. M., Ying, S.-C., Hugli, T. E., Siegel, J. N., Potempa, L. A., Jiang, H., Houghten, R. A. & Gewurz, H. (1989). *Biochemistry*, **28**, 9840–9848.
Kraulis, P. J. (1991). *J. Appl. Cryst.* **24**, 946.
Laskowski, R., MacArthur, M. W., Moss, D. S. & Thornton, J. M. (1993). *J. Appl. Cryst.* **26**, 283–291.
Lund, V. & Olafsen, J. A. (1998). *Dev. Comput. Immunol.* **22**, 185–194.
Mullenix, M. C. & Mortensen, R. F. (1994). *Mol. Immunol.* **31**, 615–622.
Myles, D. A. A., Rule, S. A., DeLucas, L. J., Babu, Y. S., Xu, Y., Volanakis, J. E., Bugg, C. E., Bailey, S. & Greenhough, T. J. (1990). *J. Mol. Biol.* **216**, 491–496.
Nicholls, A. & Honig, B. (1992). *GRASP: Graphical Representation and Analysis of Surface Properties.* Columbia University, New York, USA.
Pepys, M. B. & Berger, A. (2001). *Br. Med. J.* **322**, 4–5.
Pepys, M. B., Dash, A. C., Fletcher, T. C., Richardson, N., Munn, E. A. & Feinstein, A. (1978). *Nature (London)*, **273**, 168–170.
Potempa, L. A., Maldonado, B. A., Laurent, P., Zemel, E. S. & Gewurz, H. (1983). *Mol. Immunol.* **20**, 1165–1175.
Potempa, L. A., Siegel, J. N. & Gewurz, H. (1981). *J. Immunol.* **127**, 1509–1514.
Redinbo, M. R. & Yeates, T. O. (1993). *Acta Cryst.* D**49**, 375–380.
Rees, D. C. (1980). *Acta Cryst.* A**36**, 578–581.
Robey, F. A. & Liu, T.-Y. (1981). *J. Biol. Chem.* **256**, 969–975.

Shrive, A. K., Cheetham, G. M. T., Holden, D., Myles, D. A. A., Turnell, W. G., Volanakis, J. E., Pepys, M. B., Bloomer, A. C. & Greenhough, T. J. (1996). *Nature Struct. Biol.* **3**, 346–354.
Shrive, A. K., Holden, D., Myles, D. A. A. & Greenhough, T. J. (1996). *Acta Cryst.* D**52**, 1049–1057.
Shrive, A. K., Metcalfe, A. M., Cartwright, J. R. & Greenhough, T. J. (1999). *J. Mol. Biol.* **290**, 997–1008.
Szalai, A. J., Agrawal, A., Greenhough, T. J. & Volanakis, J. E. (1999). *Clin. Chem. Lab. Med.* **37**, 265–270.
Swanson, S. J., Mullenix, C. & Mortensen, R. F. (1991). *J. Immunol.* **147**, 2248–2252.
Thompson, D., Pepys, M. B. & Wood, S. P. (1999). *Struct. Fold. Des.* **7**, 169–177.
Volanakis, J. E. (1982). *Ann. NY Acad. Sci.* **389**, 235–250.
Volanakis, J. E. (2001). *Mol. Immunol.* **38**, 189–197.
Volanakis, J. E., Clements, W. L. & Schrohenloher, R. E. (1978). *J. Immunol. Methods*, **23**, 285–295.
Volanakis, J. E. & Kaplan, M. H. (1971). *Proc. Soc. Exp. Biol. Med.* **136**, 612–614.
Yeates, T. O. (1997). *Methods Enzymol.* **276**, 344–358.
Young, N. & Williams, R. E. (1978). *J. Immunol.* **121**, 1893–1898.